Al_2O_3 decorated with polyhedral silsesquioxane units: an unconventional filler system for upgrading thermal conductivity and mechanical properties of rubber composites

Lorenzo Mirizzi[1], Massimiliano D'Arienzo[1], Roberto Nisticò[1], Giulia Fredi[2], Sandra Diré[2,3]*, Emanuela Callone[2,3], Andrea Dorigato[2], Luca Giannini[4], Silvia Guerra[4], Silvia Mostoni[1], Barbara Di Credico[1] and Roberto Scotti[1]*

[1] Dept. of Materials Science, INSTM, University of Milano-Bicocca, Via R. Cozzi 55, 20125 Milano, Italy;
[2] Dept. Industrial Engineering, University of Trento, via Sommarive 9, 38123 Trento Italy;
[3] "Klaus Müller" Magnetic Resonance Lab., DII, University of Trento, via Sommarive 9, 38123 Trento Italy;
[4] Pirelli Tyre SpA, Viale Sarca 222, 20126 Milano, Italy.

Abstract

The present study reports on the development and exploitation of an original filler system, based on alumina nanoparticles (NPs) and polyhedral silsesquioxane (POSS) units, namely Al_2O_3@POSS, where the remarkable compatibilization and thermomechanical features imparted by the silsesquioxane cage units "makes an alliance" with the enhanced thermal conductivity of Al_2O_3 NPs. The target is to supply rubber nanocomposites with improved heat transport and mechanical properties potentially applicable in tires formulation.

The hybrid filler was prepared by a double-step approach consisting of a first silanization of Al_2O_3 with a methacrylate silane and subsequent grafting of OctaMethacrylPOSS through a radical reaction mediated by dicumyl peroxide as radical initiator. The material was characterized in depth in terms of structure, surface, and morphology and then used for producing, by *solvent-casting* technique, polybutadiene composites. The idea is to supply and test a model alumina-rubber based system which allows to better unveil the role played by the silsesquioxane units, thanks to the absence of other components (i.e. rubber polymers, vulcanization curatives and filler) usually included in real rubber formulations for tires.

The comprehensive thermomechanical and morphological characterization of the nanocomposites highlighted the key role played by POSS units decorating the alumina surface, which assure both the compatibility between filler and polymer host, and an homogeneous distribution and continuous networking of the alumina NPs. This positively influences not only the heat transport, providing thermal conductive pathways that raise the thermal diffusivity even at low filler loadings (+ 60-70 % with respect to composite enclosing bare alumina at a concentration of 15-10 v/v %) but also the storage modulus, paving the way toward a potential exploitation of Al_2O_3@POSS hybrid filler in large-scale formulations of rubber composites, namely those employed for tires.

Introduction

As promising and versatile alternatives to the traditionally applied metal-based materials, thermal conductive polymer composites are currently dominating the efforts of many researchers trying to upgrade the thermal transport efficiency in technological systems. [1]

In particular, their lightweight, easy processability, design freedom, and relatively low cost, make them potentially attractive in a number of large-scale industrial applications ranging from aeronautics, medical devices, photonics, optoelectronics, computer/electronics, to automotive. [2] However, polymers and polymer composites possess an intrinsic low thermal conductivity (*k*), [3] which severely limits their employment when fast and effective heat dissipation is necessary, like in strategic materials such as rubber composites for tires. [4] Yet, tires, working under dynamic service conditions, experience remarkable low-frequency mechanical deformations as a result of internal friction phenomena occurring at the molecular level between filler–filler, filler–rubber, and rubber–rubber units. This induces a significant heat build-up, scarcely dissipated by the low thermal conductive elastomeric matrix. [1, 5, 6]

Mitigation strategies of tire overheating effects, besides involving experimental and modelling studies, require an in-depth investigation of the rubber formulation components and, notably, on the possibility to exploit high thermally conductive fillers. Going through the reports dealing with tires application, carbon-based fillers such as graphite [7]–[9], carbon nanotubes [10]–[13], graphene [14]–[19], and carbon fibers [20] have been mainly utilized in addition to conventional carbon black, for imparting satisfactory heat transfer ability to rubber polymers, owing to their high *k* values (100-4000 W m^{-1} K^{-1} [21]–[23]) along the in-plane direction. For the efficient heat transport, filler alignment is often required, even though tailored networking, essential for assuring anisotropic thermal conductivity properties, is not so easy to attain.

Although displaying lower *k*, ceramics like Al_2O_3 [24], [25], SiC [26], [27], AlN [28], [29], and BN [30], can represent valid options in terms of availability, performance, and economic affordability. The possibility of modulating their structure, particle shape, size, and surface features have demonstrated to readily build up thermal conductive pathways within several rubbery matrices, supplying a decisive upgrade in the heat transfer [24-30].

Among these filler materials, Al_2O_3 emerges as an appealing choice, due to its low cost, stable chemical performance, and negligible toxicity, which compensate for the modest intrinsic *k*. [31] By proper tuning its crystal phase, morphology, and surface properties, alumina has been widely used as filler mostly in silicon rubber nanocomposites, endowing improved thermal conductivity as well as good mechanical and electrical insulation properties. [32]

Nevertheless, several scientific and technological problems arise upon the inclusion of Al_2O_3 in polymers, which prevent the composites to reach *k* values as high as the theoretical prediction. These are generally associated to: i) the weak interfacial adhesion between fillers and polymer chains, causing severe phonon scattering and resulting in large interfacial thermal resistance; [33] ii) the discontinuous filler distribution in the polymer matrix, which hinders the generation of thermally conductive pathways, increasing the contact thermal resistance. [6] Besides, high Al_2O_3 loadings (even higher than 50-60 v/v %) are usually required to gain a substantial enhancement in the thermal conduction, causing heavy drawbacks, i.e. viscosity increase, filler agglomerations and reduction of strength, flexibility, and processability of the composites. [34]

When dealing with rubber composites for tires, there is also the additional argument that the chemistry of alumina is significantly different compared to the ones of SiO_2 and silicate filler, currently utilized in combination with CB in tires and whose modulation is proved to impart remarkable performances [35, 36]. In fact, the lower amount of surface hydroxyl groups available at the alumina surface generally hinders its functionalization, envisaging compatibilization and segregation concerns upon incorporation in rubber matrix. This is reasonably connected to the higher crystallization temperatures required for obtaining alpha or gamma phases (> 1000 °C) that are desirable to guarantee high thermal conductivity values [34]. Other

differences may be ascribed to the presence of surface acidic sites, as opposed to the silanols at silica surface, which remarkably affect the adsorption properties of alumina [ref].
Keeping in mind all these issues, the possibility of producing Al_2O_3-rubber composites with improved thermal conductivity and satisfactory mechanical properties, simultaneously, remains a challenging task to address.
With this aim, the present work proposes the preparation and the exploitation of a filler system based on Al_2O_3 decorated at the surface with polyhedral silsesquioxane (POSS) units, able to enhance both the reinforcement and the thermal transport properties of rubber composites.
POSS, a unique family of hybrid inorganic-organic molecules with $[RSiO_{1,5}]_n$ general formula and composed of a rigid core of cage-like silicon oxide and a shell of tailorable R organic groups, exhibit or impart, when included in polymers, a number of desirable properties, e.g. outstanding thermal stability, low dielectric constant, relevant mechanical properties, chemical resistance, and biocompatibility. [37]
Very few attempts are present in the literature regarding the application of POSS in thermally conductive composites. In these studies, essentially dealing with silicone rubber composites enclosing BN [38], [39] and SiC [40] functionalized or blended with POSS molecules, nanocages have not any definite role but just the ability to improve the dispersion and the compatibilization of the filler in the rubbery matrix.
Our group has also widely investigated the properties of silsesquioxanes in polymer composites and, in particular, of OctaMethacrylPOSS units in conjunction with SiO_2 (i.e. SiO_2@POSS hybrid filler). Rubber composites for tire application with relevant reinforcement and decreased energy loss under strain were produced, suggesting the possibility to extend this strategy also to other functional materials. [41-43]
In the present study, not only alumina and POSS are used for the reinforcement of rubber, but the two materials are herein combined to develop a new hybrid filler, Al_2O_3@POSS, where the optimal compatibilization and thermomechanical features imparted by the silsesquioxane are synergistically integrated with the thermal conductivity of alumina.
Al_2O_3@POSS was synthesized by silanization of commercial Al_2O_3 with a methacrylsilane (MPTMS) and successive grafting of low loadings of POSS *via* a surface reaction assisted by dicumylperoxide (DCP), which allows both the anchoring of the nanocages and the preservation in the final hybrid structure of unreacted methacrylic functionalities, still accessible for interaction with the polymer host.
The structural, surface, and morphological features of functionalized alumina NPs were extensively investigated by spectroscopic, morphological and thermogravimetric analyses.
Al_2O_3@POSS NPs were then used to prepare, by *solvent-casting*, polybutadiene (PB) composites. The idea is to supply and test a model alumina-rubber based system that allows to better unveil the role played by the silsesquioxane units, thanks to the absence of other polymers, vulcanization curatives and filler usually required in the formulation of real rubber composites for tires.
Solid-state NMR, scanning electron microscopy (SEM), and dynamic mechanical thermal analysis (DMTA) were employed to explore the structure, morphology, and mechanical properties of PB/Al_2O_3@POSS. Finally, a comprehensive investigation of the thermal conductive properties has been performed by Laser Flash Analysis (LFA), focusing on the effect of POSS incorporation on the *k* value enhancement.
The results highlight that even at very low fillers loadings (i.e. 15-20 v/v %) remarkable heat transport and mechanical reinforcement can be achieved, suggesting potential large-scale applications.

Experimental

Materials

Al_2O_3@POSS synthesis: Alumina NanoArc, AL-0405, 99.5% (average density = 3.65 g cm^{-3}) was purchased from AlfaAesar; OctaMethacrylPOSS (POSS) from Hybrid Plastics; 3-(Trimethoxysilyl)propylmethacrylate 98% (MPTMS) and DCP from Sigma-Aldrich. *Al_2O_3/PB composites*: azobisisobutyronitrile (AIBN) and polybutadiene *cis* average M_w 200000-300000 (PB) were purchased from Sigma–Aldrich and used as received. Toluene (99.9%), used as solvent, was purchased from Aldrich.

Preparation of Al_2O_3@POSS NPs

Al_2O_3@POSS filler was prepared according to a double-step functionalization procedure previously developed for silica NPs [41] and here extended to alumina (Scheme 1).

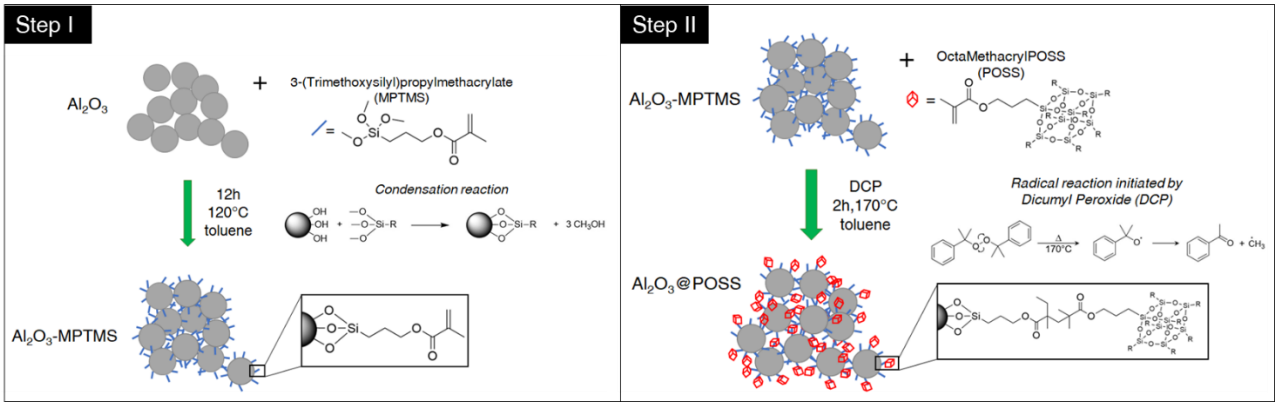

Scheme 1: Experimental procedure for the double-step preparation of Al_2O_3@POSS filler.

In the first step (Scheme 1, left), in a two-neck round-bottom flask, Al_2O_3 NPs (1.00 g) were dispersed in 25.0 mL of toluene by ultrasonication (2 min) and the mixture was brought under reflux conditions. MPTMS (0.304 g) was added dropwise to the dispersion and the reaction mixture was kept under reflux conditions and stirred vigorously. After 12 h, the mixture was centrifuged at 9000 rpm for 15 min and washed twice with toluene and ethanol. Finally, Al_2O_3-MPTMS NPs were put in an oven at 120 °C for 12 h.
Successively, Al_2O_3-MPTMS NPs were suspended in toluene (50.0 mL) and then POSS (0.1000 g) was introduced into the solution. A small amount of DCP (4 wt. % with respect to Al_2O_3-MPTMS) was added and the suspension was refluxed at 170°C for 2 h. The peroxide decomposes at ~ 168 °C generating free radicals that promote the activation of the methacrylate groups of both MPTMS and POSS, favoring the grafting of the nanocages onto the functionalized alumina surface (Step II, Scheme 1).

The obtained Al_2O_3@POSS powders were filtered, washed several times with toluene and finally with EtOH, and dried in at 120 °C for 12 h.

Preparation of PB/Al_2O_3 composites

Bare Al_2O_3, Al_2O_3-MPTMS, and Al_2O_3@POSS NPs were incorporated into PB to produce composites, according to the procedure shown in Scheme 2.

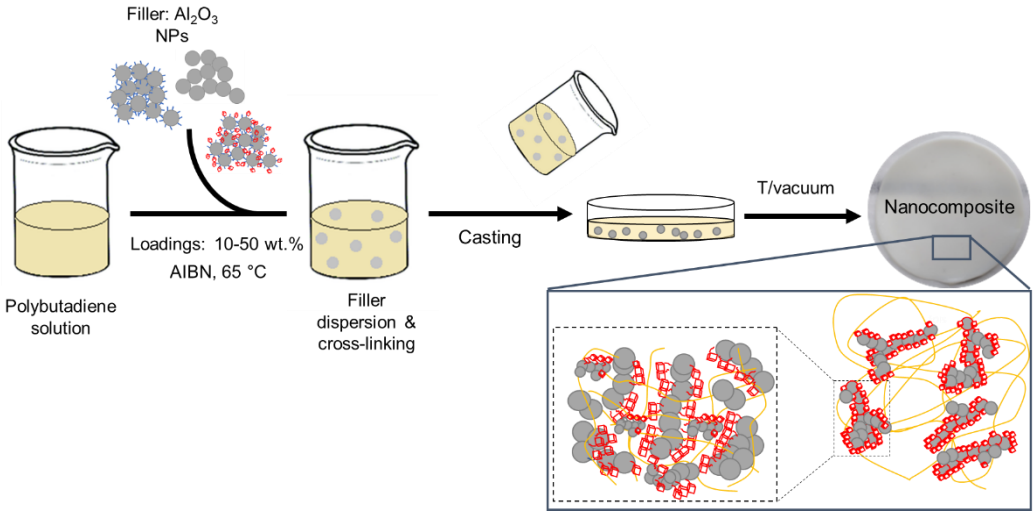

Scheme 2. Experimental procedure for the preparation of PB/alumina composites by *solvent-casting*.

Pre-dried PB (2.0 g) was dissolved in 20.0 mL of anhydrous toluene at 65 °C. Then, different filler loadings (10, 30, 40, 50 wt%, corresponding to 2.57, 9.24, 13.67, 19.19 v/v %, respectively) and AIBN (0.02 g) were added simultaneously to the hot polymer solution and stirred at 65 °C for 6 h under N_2 flow.
AIBN should promote the networking among Al_2O_3@POSS particles to form larger and interconnected aggregates as a result of reactions of the acrylate groups, as well as reactions of the pending acrylate functions of POSS units of the hybrid filler with suitable C═C double bonds of the PB matrix.
The dispersions were cast in Teflon Petri dishes and the volatiles were removed overnight by maintaining the system under an aspiration hood. Complete elimination of the by-products was achieved by heating the samples at 70 °C for 9 h. The samples were stored under N_2, to avoid any possible contamination. Self-standing composites with an average thickness of 280–300 μm were finally obtained.
Hereafter, the nanocomposites will be labeled PB/XAl_2O_3Y where X refers to the different percentage of filler (X= 10, 30, 40, 50 wt%), while Y denotes the different surface functionalization (Y = -MPTMS, @POSS). As a reference material, 2.0 g of PB were dissolved in toluene and the same experimental procedure for the preparation of nanocomposites was followed.

Materials Characterization

Powder X-ray diffraction (PXRD) patterns were collected with a Rigaku Miniflex 600 diffractometer (Cu Ka radiation) in the 2θ range 10-80 ° (2θ step 0.020 °, 1 ° min^{-1} scan rate).
To preliminarily check the alumina functionalization with MPTMS and, successively, with POSS, ATR-FTIR measurements were performed on a Thermo Fisher Nicolet iS20 FTIR spectrometer (1 cm^{-1} resolution spectra, 525–4000 cm^{-1} region, 16 scans). To quantitatively assess the MPTMS and POSS grafting onto alumina surfaces, Thermo Gravimetric Analysis (TGA) measurements before and after the double-step functionalization procedure were performed. TGA thermograms were collected by a Mettler Toledo TGA/DSC1 STARe System, at a constant gas flow (50 cm^3 min^{-1}). The sample was previously taken into the furnace to 150 °C for 15 min to remove humidity and any residual solvent and subsequently heated at a rate of 10 °C min^{-1} up to 1000 °C.
Elemental composition of the samples was determined by using CHNS Analyzer Elementar VarioMICRO.
The structure of Al_2O_3@POSS nanofiller was characterized by solid-state NMR. Analyses were carried out with a Bruker 400WB spectrometer operating at a proton frequency of 400.13 MHz under the following conditions: ^{27}Al frequency: 104.67 MHz, π/12 Hahn-echo pulse length 2.2 μs, 3 s recycle delay, 1k scans. ^{29}Si frequency: 79.48 MHz, single pulse sequence: π/4 pulse 3.9 μs, recycle delay 300s, 1k scans. ^{13}C frequency: 100.48 MHz, contact time 2 ms, decoupling length 5.9 μs, recycle delay: 3 s, 5 k scans. Samples were packed in 4 mm zirconia rotors, which were spun at 11 or 8 kHz, under air flow. $Al(NO_3)_3$(aq) 1M, adamantane and Q8M8 were used as external secondary references. The Si structural units are labelled according to the usual NMR notation: T^n indicates R-SiO_3 silicon units and n is the number of oxo-bridges. Bruker TopSpin software was used for the line shape analysis. The results were considered acceptable with a confidence level of 95%.
Morphological characterization of Al_2O_3 and Al_2O_3@POSS powders was performed on the transmission electron microscope (TEM) Jeol JEM-2100Plus operating at 200 kV (0.24 nm point-to-point resolution). The powders were suspended in ethanol, and a drop of this suspension was deposited on a 3 nm carbon film supported on copper grid for TEM investigation.
The morphological features of PB/alumina composites were investigated by scanning electron microscopy (SEM) measurements on a Zeiss Gemini 500 microscope equipped with a standard secondary electron detector and the Bruker Quantax detector for EDS (Energy Dispersive) microanalysis. SEM images were collected on very tiny portions of PB films, that were deposited over carbon tape onto suitable SEM stubs. Graphite coating was performed to increase the sample conductivity. To get the best reliability from the investigation, at least 10 images for each nanocomposite in different sample region were acquired.

The microscopic morphology of the composites was also studied by Atomic Force Microscope (AFM, Bruker Veeco Dimension 3100) operating in tapping mode in air and by Transmission electron microscopy (TEM) images by using a Jeol JEM-2100Plus operating at 120 kV.

Solid state NMR analysis has been also applied with a Bruker 400WB spectrometer under the following conditions: ^{1}H at 400.13 MHz $\pi/2$ pulse 3.9 μs, recycle delay 5s, 16 scans. Relaxation studies though $T^{H}_{1\rho}$ and T_2 were done with spin-lock pulse sequence with a variable spin-lock pulse in the range 0.5 – 500 ms (frequency field 20 kHz was used for the spin-lock field B1) [44] and cpmg sequence setting the echo time between 8 and 2000 ms [45], respectively.

TGA was performed to study the thermal properties of the composites. TGA thermograms were collected by using a Mettler Toledo TGA/DSC1 STARe system at constant gas flow (50 cm^3 min^{-1}). The sample powders were heated in air from 30 to 1000 °C at a rate of 10 °C min^{-1}.

DMTA measurements were carried out by a DMA Q800 apparatus from TA Instruments (New Castle, DE, USA) in tensile mode. A rectangular specimen (gauge length of 12 mm; pre-stress of 0.01 N; sinusoidal strain with a frequency of 1 Hz and amplitude of 0.05 %) was first cooled from room temperature to -120 °C at a rate of 5 °C/min and then heated up to 100 °C at a heating rate of 3 °C/min. Storage modulus and loss modulus were measured and compared as a function of temperature.

The thermal diffusivity and conductivity of the prepared composites were determined via a light flash analyzer LFA 467 (Netzsch Holding Gmbh, Selb, Germany). Tests were performed at 25 °C on discoidal specimens with a diameter of 12.7 mm, die cut from the prepared composites, and coated with a graphitic spray on both sides. In order to assure the reproducibility of the performances and to assess the uncertainty on the measurement, at least two specimens per composition, taken from composites obtained from different preparations, were tested and at least five pulses were performed on each specimen. Data were analyzed with the embedded software Proteus® by applying a transparent model with linear baseline and numerical pulse correction. These tests allowed the direct measurement of the thermal diffusivity (α). Then, the thermal conductivity at 25 °C (k) was calculated via Equation (1):

$$k = \alpha \cdot \rho \cdot c_p \quad (1)$$

where ρ is the pycnometer density (at 23.0 °C) and c_p is the specific heat calculated via differential scanning calorimetry (DSC) by following the standard ASTM E1269-11.

Results and Discussion

Structural, morphological and surface characterization of alumina-based fillers

The structural features of commercial Al_2O_3 powders were investigated by XRD (see Fig. S1 in Supporting Information, SI). The diffraction pattern evidences the co-existence of two different crystalline structures, i.e. γ and δ alumina (JCPDS card no. 29-0063 and JCPDS card no. 46-1215, respectively) as well as the occurrence of other peaks, probably related to impurities. The phase composition of the sample, determined by profile fitting, resulted ~88% of γ– Al_2O_3 and ~12 % of δ–Al_2O_3.

To verify the effective functionalization of alumina NPs with MPTMS and, subsequently, with POSS molecules, FT-IR analysis was performed. Figure 1 reports the comparison among the spectral features of pristine POSS, Al_2O_3@MPTMS, and Al_2O_3@POSS.

As expected, the spectra of Al_2O_3-MPTMS and Al_2O_3@POSS (blue and red lines, respectively) are rather similar, since the organic functional groups of MPTMS and POSS are basically the same. In fact, the C═O and C═C stretching modes of the methacrylic groups at 1710 and 1640 cm^{-1}, respectively, and the peaks at about 2940 and 2860 due to the C-H stretching of the CH_2 groups (insets in Fig. 1) are evident in both the functionalized samples, compared to bare Al_2O_3 (Fig. S2 in the SI). Besides, the occurrence of an intense band at 1090 cm^{-1} related to the Si–O stretching vibration typical of the POSS cages, indicates the presence of the silsesquioxane units on the filler surface.

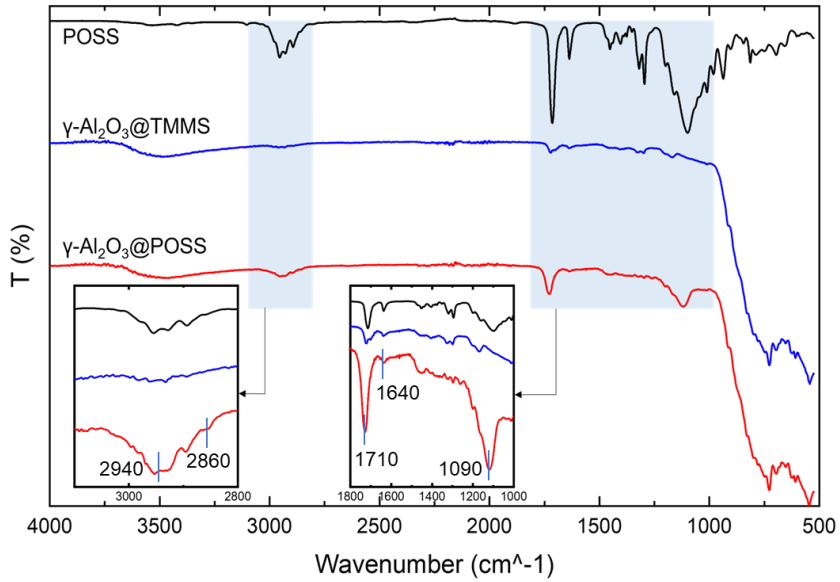

Figure 1 – FT-IR spectra of: pure POSS (black line), Al_2O_3-MPTMS (blue line) and Al_2O_3@POSS (red line); the insets show the magnifications of the spectral regions related to the functional groups of POSS units.

To quantitatively evaluate the functionalizing agents anchored on the Al_2O_3 surface, TGA analysis was performed. In detail, the thermal profiles of Al_2O_3, Al_2O_3-MPTMS, and Al_2O_3@POSS NPs are reported in Figure 2. Bare alumina (black curve) shows a very small weight loss above 400 °C, which was associated to the condensation of surface Al-OH groups with the consequent release of water. The amount of MPTMS grafted onto the alumina surface in Al_2O_3-MPTMS was calculated from the net weight loss between 150 and 1000 °C. The contribution of bare alumina due to unbonded surface hydroxyl groups was calculated and subtracted from the net weight loss. Using the same protocol and subtracting the contributions of both bare Al_2O_3 and MPTMS from the total weight loss, the amount of POSS units in Al_2O_3@POSS was estimated.
Assuming that the functionalizing agents were equally distributed on the oxide surface and referring to the specific surface area of alumina provided by the supplier (SSA_{BET} = 35 $m^2\ g^{-1}$), the grafted amount (mmol g^{-1}) and the number of functionalizing molecules per nm^2 (σ = molecules nm^{-2}) for each system were evaluated and reported in Table 1.

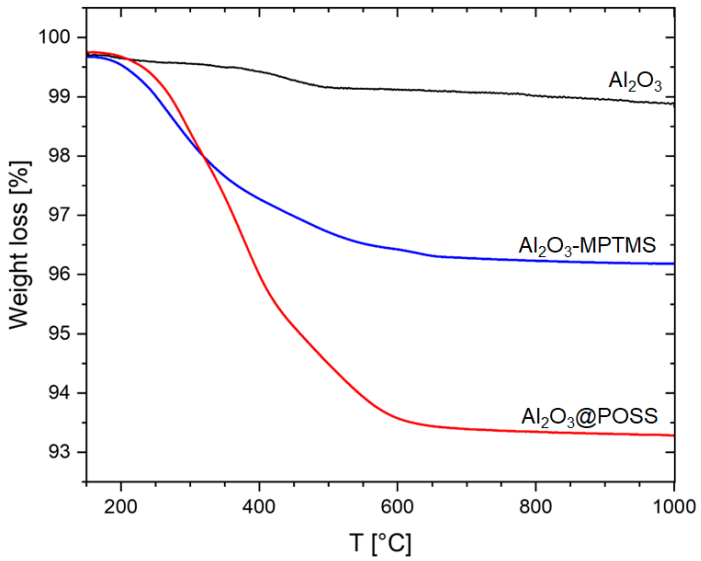

Figure 2 – TGA curves of bare Al_2O_3 (black line), Al_2O_3MPTMS (blue line) and Al_2O_3@POSS (red line).

Table 1- Surface density of functional molecules on Al_2O_3-MPTMS and Al_2O_3@POSS (σ).

Sample	Net weight loss 150-1000 °C (wt. %)	M_w (g mol^{-1})	Grafted amount (mol g^{-1})	σ (molecules nm^{-2})
Al_2O_3-MPTMS	2.13	248.4	$1.41 \cdot 10^{-4}$	2.7
Al_2O_3@POSS	5.04	1434.0	$4.17 \cdot 10^{-5}$	0.8

Further insights into the surface modification with MPTMS and POSS was provided by solid state NMR. The ^{29}Al spectra of Al_2O_3, Al_2O_3-MPTMS, and Al_2O_3@POSS samples are reported in Figure S3 (See Supporting Information). For all the samples the main peak at 7.7 ppm is assigned to octahedral Al sites (i.e. Al(VI)) and the minor component at about 59 ppm is attributed to tetrahedral Al atoms (i.e. Al(IV)) [45-48] . The spectra are perfectly superimposable with the ratio Al(IV)/Al(VI) = 28:72, confirming that the functionalization processes do not alter the Al-O structure.

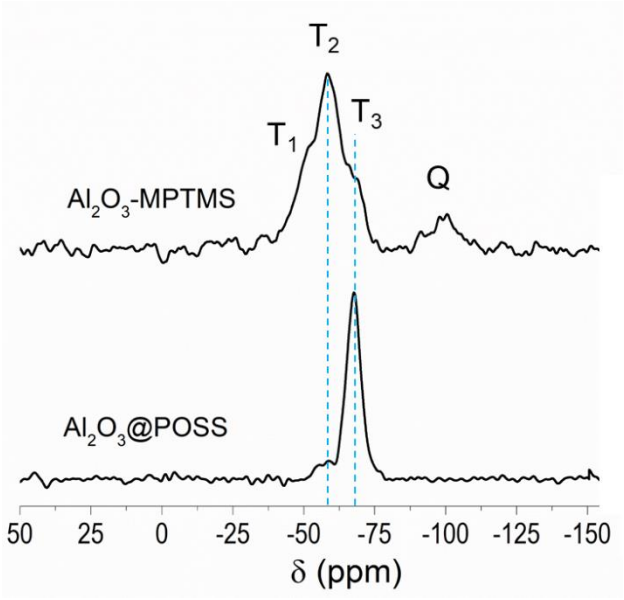

Figure 3 – ^{29}Si CPMAS spectra of Al_2O_3-MPTMS and Al_2O_3@POSS.

By CPMAS ^{29}Si NMR investigation, a remarkable difference can be outlined between the functionalized alumina samples (Figure 3). Al_2O_3-MPTMS spectrum shows the T^1, T^2 and T^3 units due to the organosilane at δ -45.5, -54.7, and -64.3 ppm, respectively. The small amount of Q units at about 100 ppm is due to the declared silica impurity present in the commercial alumina sample. Although the CPMAS is semi-quantitative and the Si-OH units are strongly favoured with respect to Si-O-Si one, it could be noted that the presence of both T^2 and T^1 units indicates an incomplete silane condensation. Instead, the Al_2O_3@POSS spectrum displays the presence of a sharp signal ascribable to fully condensed T^3 units at -66.3 ppm, together with a small amount of T^2. The resonances belong both to POSS and MPTMS because they originate superimposable signals due to their identical Si neighbourhood. Nevertheless, the T_3 component is here dominated by the POSS units, since there are eight silicon atoms (of the type $RSi(OSi)_3$) per cage in every POSS unit. However, the presence of MPTMS in this spectrum can be deduced by the T_2 shoulder.

To gain information on the interactions among the acrylate functions of MPTMS and POSS, thus supporting the silsesquioxane grafting onto the alumina surface, ^{13}C CPMAS NMR investigation was performed (Figure 4). The liquid NMR spectrum of MPTMS and the corresponding labelling is also reported for comparison (Figure 4, top). Both Al_2O_3-MPTMS and Al_2O_3@POSS do not show the occurrence of O$\underline{C}H_3$ resonance at 50 ppm (8 in MPTMS), suggesting a fully hydrolysed organosilane. Moreover, the downfield chemical shift of *7* (Si-$\underline{C}H_2$-) is an index of condensation.

For Al_2O_3-MPTMS sample, the presence of new weak signals (*1a, 2a*) in the 60-40 ppm range, together with all the typical MPTMS peaks, indicates that a partial polymerization occurred. It is confirmed by the broadening and downfield shift of *4* , compared with the sharp peak of the pristine MPTMS at 167 ppm.[41] Since the δ C=O group is very sensitive to the environment, a distribution of both polymerized and not (*4a*, *4*) methacrylate functions can be argued from its broadness. Instead, the carbon spectrum of the POSS organic tail indicates highly but not complete polymerized units, due to the residual peaks *1* and *2,* belonging to unreacted methacrylate functionalities, and the intense peak *2a* together with the downfield shift of *4* (175.8 ppm). Moreover, all the resonances are broader than in MPTMS, indicating a more rigid system.

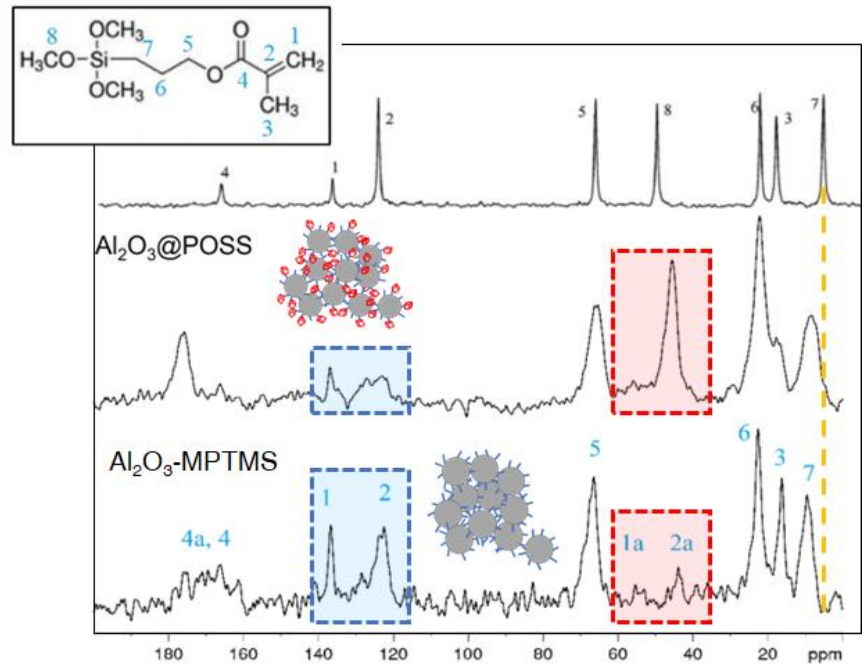

Figure 4 – ^{13}C CPMAS NMR spectra of Al_2O_3-MPTMS and Al_2O_3@POSS. For comparison, the liquid NMR spectrum of the pristine MPTMS is also reported (top). Labels *1a,2a* and *4a* refer to the new methylene units due to polymerization and the vicinal carbonyl, respectively.

In summary, solid-state NMR analysis confirms the effective surface functionalization of alumina with POSS units, demonstrating the validity of the double-steps approach. In fact, by the suggested protocol, when alumina is first functionalized with the silane (Al_2O_3@MPTMS), only a partial self-polymerization of MPTMS terminations occurs and free methacrylate groups remain still available for the cross-linking reaction with POSS chains. This may surely limit the POSS grafting yield, but it makes easier the control of the reaction at the surface of alumina NPs. Finally, the presence in Al_2O_3@POSS of methacrylate groups of both POSS and MPTMS still accessible for the cross-linking reaction with PB chains, indicates the suitability of the hybrid filler in supplying enhanced networking/interaction with the polymeric matrix.

The morphological features of Al_2O_3@POSS NPs were explored by TEM and compared to that of bare nanosized alumina (Figure 5). The commercial alumina is composed of polydisperse spherical NPs with average diameters ranging from 20 to 150 nm (Fig. 5a). At higher resolution, besides some necking among the NPs, crystalline planes and clearly defined edges can be detected (Fig. 5b). After functionalization with POSS, the NPs boundaries appear less defined than in naked alumina (Fig. 5c, d). This behaviour may reasonably suggest the presence of POSS domains, which create a surface shell on the alumina surface, in line with the previously reported spectroscopic investigation.

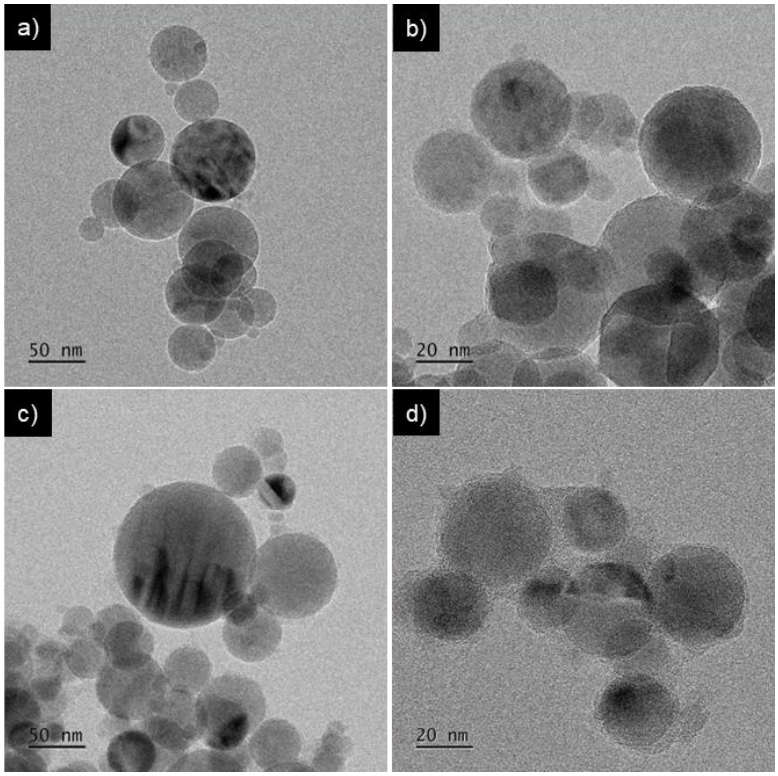

Figure 5 – TEM images of Al_2O_3 (a, b) and Al_2O_3@POSS (c, d) NPs.

Spectroscopic and morphological characterization of nanocomposites

The influence of alumina NPs incorporation on the polymer matrix was initially assessed by FTIR. In detail, Figure 6 shows as a representative example the spectra of polymerized PB, Al_2O_3@POSS, and a selected corresponding nanocomposite (i.e. PB/40Al_2O_3@POSS).

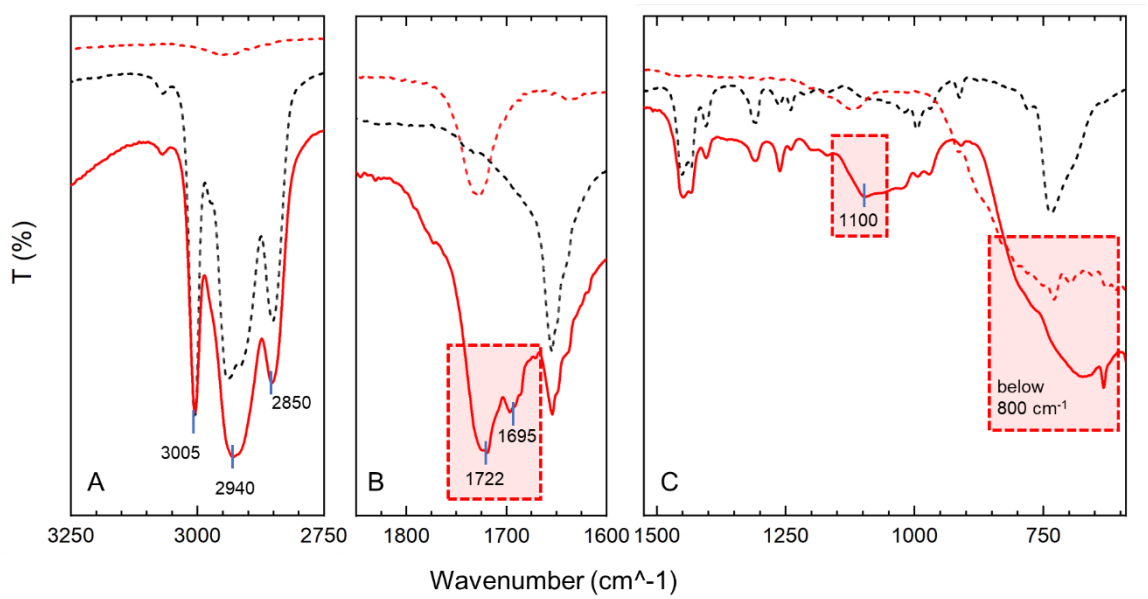

Figure 6 – FTIR spectra of Al_2O_3@POSS (red-dotted line), homopolymerized PB (black-dotted line) and PB/40Al_2O_3@POSS (red line) in the A) 2750-3250 cm^{-1}, B) 1600-1850 cm^{-1} and C) 590-1525 cm^{-1} spectral regions.

For better visualization of the absorption bands, three different spectral regions have been highlighted. In Fig. 6A, in the spectrum of PB/40Al_2O_3@POSS, it is possible to recognize the principal peaks ascribed to PB: the =C–H stretching at ~3005 cm^{-1}, the asymmetrical and symmetrical C–H stretching vibration of methylene groups at ~2940 cm^{-1} and ~2850 cm^{-1}, respectively. The filler introduction does not substantially affect the spectral features, except for a small broadening of the band at ~2940 cm^{-1}.

More relevant changes can be observed at lower wavenumbers (Fig. 6B-C). In particular, upon crosslinking in the presence of Al_2O_3@POSS, new signals at ~1695 cm^{-1} and ~1722 cm^{-1} arise (Fig. 6B). These new features can be tentatively associated to the self-polymerization of the POSS methacrylic groups. Finally, the relatively intense and broad band at ~ 1100 cm^{-1} is ascribable to the Si–O stretching vibration of the POSS cages, while in the region below 800 cm^{-1} the signal of alumina dominates the spectrum (see Fig. 6C).

Similar results have been obtained for the other PB/XAl_2O_3@POSS nanocomposites (not reported).

The filler distribution in the cured nanocomposites was comprehensively investigated by SEM-EDS analysis. As a representative example, SEM micrographs and the corresponding Al elemental mapping images collected for PB/40Al_2O_3, PB/40Al_2O_3@MPTMS, and PB/40Al_2O_3@POSS are reported in Figure 7.

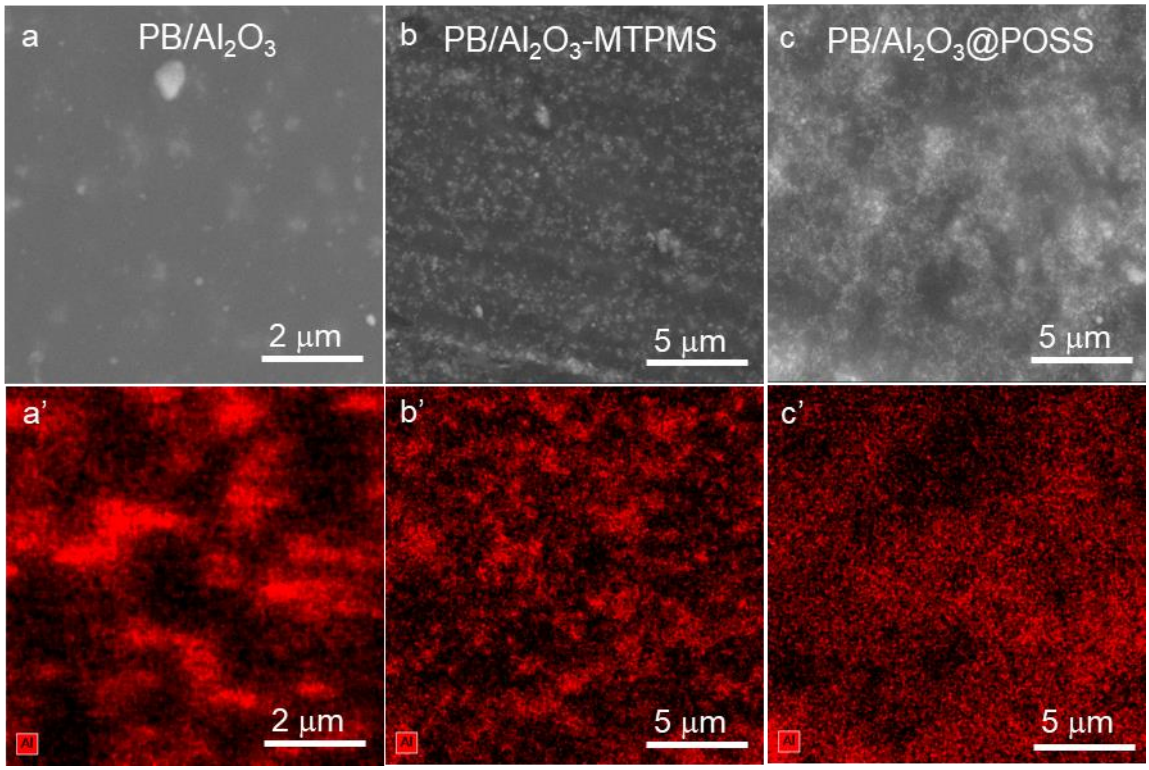

Figure 7 – SEM micrographs and corresponding EDS elemental maps of Al for PB/40Al_2O_3, PB/40Al_2O_3@MPTMS, and PB/40Al_2O_3@POSS nanocomposite samples.

The NPs organization in the polymer matrix is significantly influenced by surface functionalization. In fact, inhomogeneous and isolated filler aggregates with micrometric size are visible in the case of naked Al_2O_3 (Fig. 7a), due to the poor compatibility between polar oxide surfaces and non-polar PB chains. This behaviour is much more evident by EDS elemental map of Al (Fig. 7a').
Conversely, for PB/40Al_2O_3-MPTMS and PB/40Al_2O_3@POSS nanocomposites, the filler distribution improves, as a result of the better affinity imparted by the surface modification (Fig. 7b, c). However, some remarkable differences between the samples are noticeable. In the case of PB/40Al_2O_3-MPTMS, alumina NPs are organized in nanometric or sub-micrometric aggregates, which seem only partially connected (Fig. 7b, b').

Interestingly, when POSS nanounits decorate the filler surface, smaller nanometric aggregates homogeneously distributed in the PB matrix and likely forming a continuous and interconnected network can be observed (Fig. 7c, c'). This peculiar filler arrangement foreshadows the potential generation of thermally conductive pathways, which may enhance the heat transport in these materials.
Further proofs of the unique behavior of the hybrid filler were derived from AFM and TEM analysis of PB/10Al_2O_3@POSS composite (Fig. S4 in SI). The images, besides confirming a homogeneous dispersion and interfacial adhesion with the polymer host, show the presence of interconnected agglomerates network, even at relatively low filler loading.

To further elucidate the structural effects of alumina incorporation in PB, ^{1}H solid-state NMR relaxation experiments were performed. Figure 8 shows the proton spectra of nanocomposites. The two resonances at 2.1 and 5.4 ppm due to PB methylene and methyne units are visible. More interestingly, a clear linewidth variation among the samples can be observed with a significant broadening in the case of sample PB/40Al_2O_3@POSS. A similar linewidth increase with alumina functionalization is observed also in the ^{13}C MAS spectra (not shown). This evidence suggests evaluating the effect of the different nanofillers through the relaxation studies calculating both spin-spin (T_2) and spin-lattice in the rotating frame ($T^H_{1\rho}$) relaxation times. The values are summarized in Table 2.

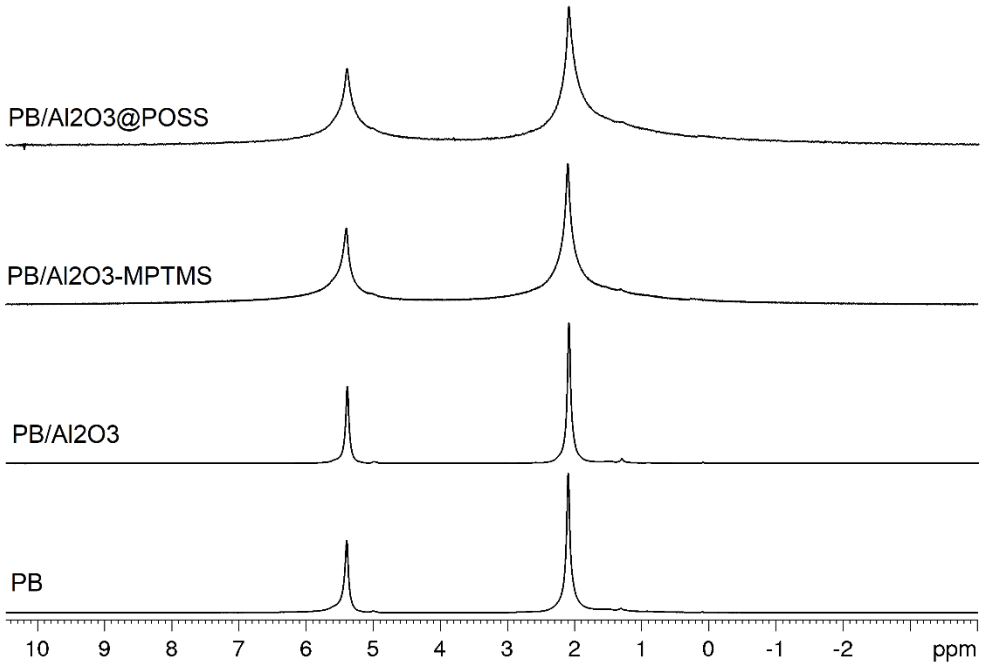

Figure 8. ^{1}H MAS spectra of homopolymerized PB and composite samples.

The linewidth of the PB resonances decreases with the addition of the bare alumina filler, whereas it increases with the functionalized filler, indicating different chain organization at the molecular level. This picture is confirmed by the relaxation experiments, since the bare alumina causes expected slightly higher $T^H_{1\rho}$ and T_2 values confirming polymer chains stiffening. The functionalized filler instead produces a strong reduction of the relaxation times, which indicates relevant molecular interactions between polymer chains and the organic groups grafted onto the alumina filler, leading to conformational reorganization of the chains. [48] The effect is more pronounced in the case of PB/40Al_2O_3@POSS with respect to PB/40Al_2O_3-MPTMS, since POSS units can interact with PB chains through a large number of organic groups (up to 7) localized on the cage, thus improving the polymer-filler interface. This description at the molecular

level is in good agreement with the homogeneous distribution of the filler highlighted by EDS map and AFM images, as well as with the mechanical properties discussed below.

Table 2. Resonance linewidth and relaxation time constants $T^{H}_{1\rho}$ and T_2 obtained from the analysis of the proton spectra and related magnetization curve trends for all the composites (values intended within ±0.2ms).

		PB	PB/40Al_2O_3	PB/40Al_2O_3-MPTMS	PB/40Al_2O_3@POSS
LW (Hz)	-CH_2-	24.0	20.2	60.4	78.9
	=CH-	25.5	19.3	56.2	81.2
$T^{H}_{1\rho}$ (ms)	-CH_2-	41.2	57.5	16.5	11.8
	=CH-	38.9	52.6	16.8	11.7
T_2 (ms)	-CH_2-	25.5	29.9	16.2	12.6
	=CH-	24.5	29.4	16.1	13.1

Functional properties of the nanocomposites: thermal diffusivity and dynamic mechanical analysis

The thermal transport properties of the nanocomposites were assessed by LFA analysis (Figure 9). In detail, Figure 9a reports the trend of the thermal diffusivity (α) as a function of the filler volume fraction for PB/Al_2O_3, PB/Al_2O_3-MPTMS, and PB/Al_2O_3@POSS.

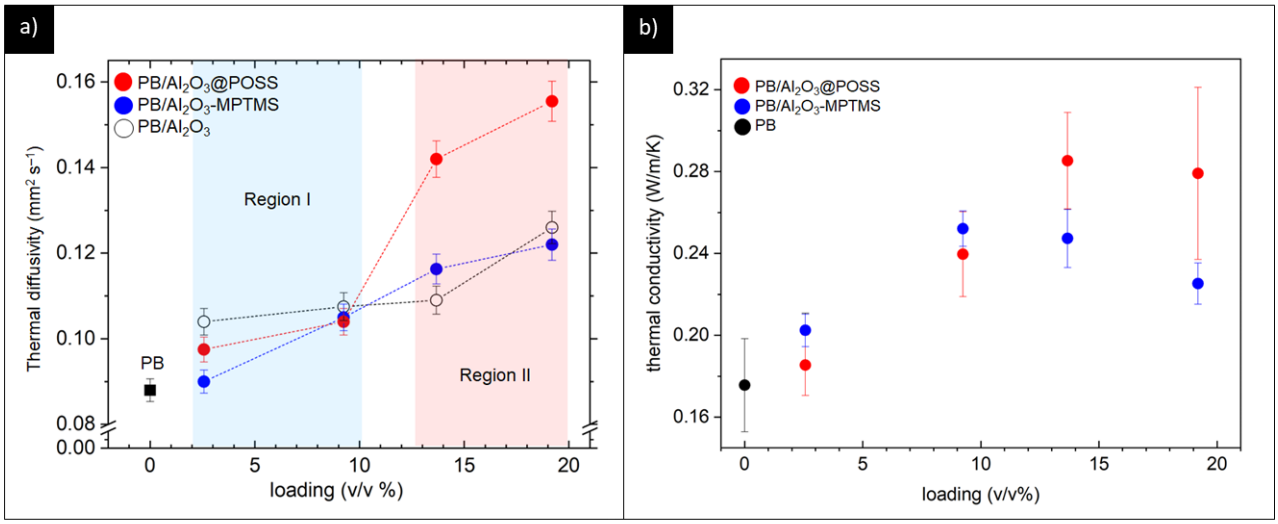

Figure 9 – Trends of thermal diffusivity (α) and thermal conductivity (*k*) for homopolymerized PB and PB filled with unmodified and functionalized Al_2O_3 NPs.

Two distinct regions can be identified. At low filler loadings (< 10 v/v %, Region I), the heat transfer properties of PB/Al_2O_3 nanocomposites generally do not undergo significant changes, whereas a slight but appreciable increase in thermal diffusivity values can be noticed in the presence of Al_2O_3-MPTMS and Al_2O_3@POSS NPs. The results suggest that, at a low filler concentration, organosilane or POSS units primarily act as compatibilizing agents, fostering the occurrence of randomly dispersed and poorly interacting NPs aggregates in the polymer matrix. This hypothesis is strengthened by the SEM-EDS images (Fig. 7a-a',b-b') of the composites in which, though referring to a higher filler loading, isolated or partially connected filler aggregates are detectable.

Upon an increase of the filler volume fraction up to ~ 20 v/v % (Region IIa noteworthy increase in the thermal transport (+ 60-70 % with respect to PB/Al_2O_3 and PB/Al_2O_3-MPTMS and + 90 % compared to homopolymerized PB) is observed for PB/Al_2O_3@POSS nanocomposites while for PB/Al_2O_3 and PB/Al_2O_3-MPTMS the thermal diffusivity is hardly altered.

This marked enhancement, occurring at rather low volume fractions if compared with similar studies reported in the literature [49, 50], again may find its origin in the morphological features of the nanocomposite, where Al_2O_3@POSS NPs appear arranged in a continuous and interconnected network in the PB matrix (Fig. 7c, c'), as a results of filler-filler and filler-polymer interaction promoted by the highly reactive POSS terminations. This peculiar arrangement seems to play a key role in supplying thermally conductive pathways while reducing the interfacial thermal resistance.

From the thermal diffusivity values, the conductivity was then calculated by the equation:

$$k = \alpha \cdot \rho \cdot C_p$$

where ρ is the density measured by He pycnometer and C_p is the specific heat capacity of the composites measured by DSC (see SI for details). Although with large standard deviations, higher *k* values are retrieved for PB/Al_2O_3@POSS composites with respect to PB/Al_2O_3-MPTMS and homopolymerized PB (Fig. 9b). Since the "raw measure" of the thermal transport (i.e. thermal diffusivity) displays small error bars and considering the low standard deviations on the density measurements by He picnometer (See Table S1 in SI), the high deviations of the *k* values observed for PB/Al_2O_3@POSS have to be attributed to the relatively large uncertainty on the determination of the C_p made by DSC. This can be connected to several parameter: i) for the analysis, very small portions of material were collected in different regions of each sample and, as polymer composites often have less than perfect geometries, small variations of shape and weight of the specimens strongly influences the accuracy of the determined C_p values; ii) local inhomogeneities in the composites cannot be excluded, especially in the presence of POSS cages, which may generate nanoporosities and voids around the filler particles decreasing the specific heat capacity.
Nevertheless, the trend of the thermal conductivity confirms once again the ability of the POSS nanounits in improving the thermal transport in PB nanocomposites.

As already mentioned, obtaining Al_2O_3-rubber composites with improved thermal transfer ability and satisfactory mechanical properties, simultaneously, is an ambitious task. In light of the good thermal transport properties evidenced by the PB/Al_2O_3-MPTMS and PB/Al_2O_3@POSS nanocomposites, DMTA analysis was performed in order to study the effect of the filler surface functionalization also on the mechanical properties.

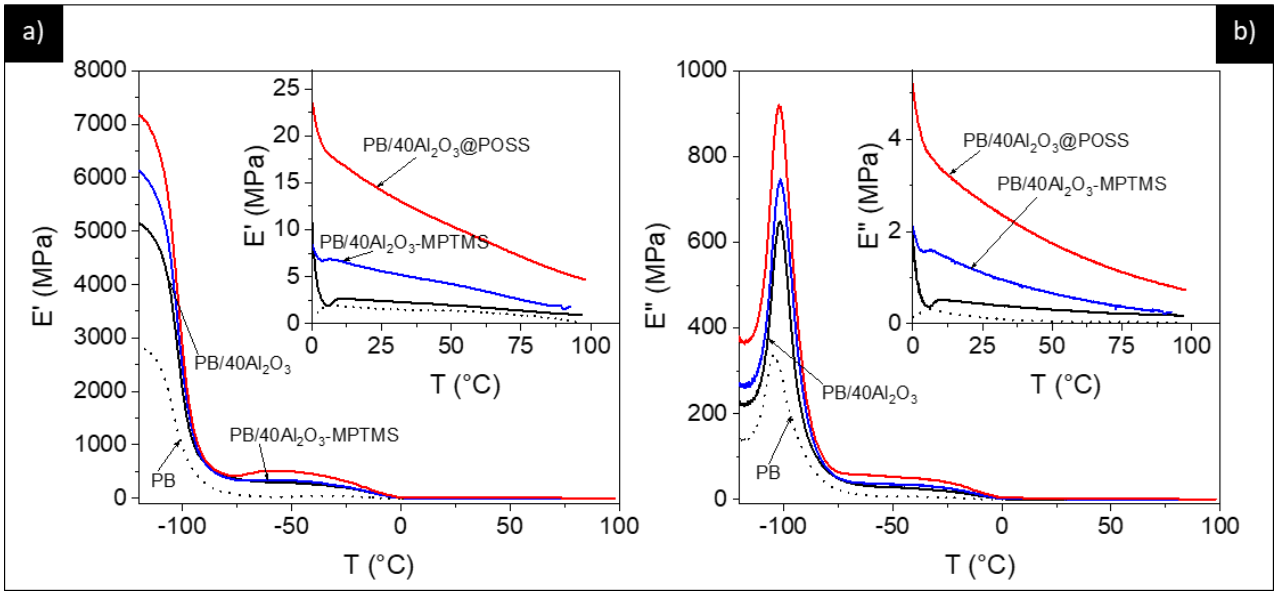

Figure 10 – Trend of the storage and loss moduli of homopolymerized PB (dotted line), PB/40Al_2O_3 (black line), PB/40Al_2O_3-MPTMS (blue line) and PB/40Al_2O_3@POSS (red line) nanocomposites.

Figure 10 shows the results of the DMTA analysis and reports the trends of the storage modulus (E') and loss modulus (E'') as a function of temperature for the neat PB and the composites with 40 wt% of filler, i.e., PB-40Al_2O_3, PB-40Al_2O_3-MPTMS, and PB-40Al_2O_3-POSS. The storage modulus decreases with increasing temperature overall the whole investigated temperature range, with the most evident drop between -110 °C and -90 °C, due to the glass transition, as also evidenced by the peak of E''. The peak temperature of E'', corresponding to the glass transition temperature (T_g), is slightly shifted to higher temperatures upon nanofiller addition, as it increases from -104 °C of neat PB to -101 °C of the nanocomposites, probably due to the confinement effect of the nanofillers on the PB chains and/or their influence on the crosslinking efficiency. On the other hand, the various surface states of the nanoparticles do not remarkably influence the T_g. What is really affected by the surface functionalization is the absolute values of E' and E'', as the addition of nanoalumina increases the values of both E' and E'' compared to those of neat PB, not only in the glassy state, but also above T_g, as observable from the inset of Figure 10a and 10b. The same trend is appreciable for E'' and may be attributed to the inhibition of the relaxation process within the composites as a consequence of the nanofiller addition [51], which is much more evident in the PB/40Al_2O_3@POSS nanocomposite.
These results indicate that tiny amounts of POSS nanocages decorating alumina surfaces, besides exerting a unique effect on the heat transport of the nanocomposites, remarkably upgrade their mechanical properties, providing a continuous network and an enhanced filler-matrix interaction.

Conclusions

An unconventional Al_2O_3@POSS hybrid filler, where alumina particles and POSS units belong to the same functional structure, was synthesized by grafting tiny amounts of OctaMethacrylPOSS onto silanized commercial alumina NPs. Upon incorporation in PB matrix, both thermal conductivity and elastic modulus remarkably increase, even at relatively low loadings of thermally conductive filler (15-10 v/v %). This effect originates from the specific structure of the hybrid filler, where the shell of POSS nanounits, besides assuring the compatibility and interaction between the filler and the polymer host at the nanoscale, imparts an homogeneous distribution and continuous networking of the alumina NPs. The promising results along with the moderately low costs of the material, foreshadow the potential application of Al_2O_3@POSS hybrid filler in large-scale formulations of rubber composites, such as those utilized for tires. In this view next steps will be aimed at promoting the scaling-up of filler production considering the possible substitution of organic solvents towards the principle of the green chemistry, to increase the process sustainability also in terms of costs and impact of the whole process.

Acknowledgements

L.M. thanks CORIMAV ("Consortium for the Research of Advanced Materials between Pirelli and Milano Bicocca University) for its support within the PCAM European Doctoral Program.

M.D. gratefully acknowledge Dr. Mattia Carnevale and Mr. Daniele Pontoriero for their support in the filler synthesis and nanocomposites characterization.

References

[1] N. Burger, A. Laachachi, M. Ferriol, M. Lutz, V. Toniazzo, D. Ruch, Review of thermal conductivity in composites: Mechanisms, parameters and theory, Prog. Polym. Sci. 61 (2016) 1–28. https://doi.org/10.1016/j.progpolymsci.2016.05.001.

[2] H. Chen, V.V. Ginzburg, J. Yang, Y. Yang, W. Liu, Y. Huang, L. Du, B. Chen, Thermal conductivity of polymer-based composites: Fundamentals and applications, Prog. Polym. Sci. 59 (2016) 41–85. https://doi.org/10.1016/j.progpolymsci.2016.03.001.

[3] Y. Xu, X. Wang, Q. Hao, A mini review on thermally conductive polymers and polymer-based composites, Compos. Commun. 24 (2021) 100617. https://doi.org/10.1016/j.coco.2020.100617.

[4] S.M. Danilova-Tret'yak, On Thermophysical Properties of Rubbers and Their Components, J. Eng. Phys. Thermophys. 89 (2016) 1388–1393. https://doi.org/10.1007/s10891-016-1506-5.

[5] S.L. Sokolov, Analysis of the heat state of pneumatic tires by the finite element method, J. Mach. Manuf. Reliab 38 (2009) 310–314. https://doi.org/10.3103/S1052618809030182.

[6] Z. Wang, Y. Lu, J. Ding, L. Zhang, T.W. Chan, Preparation of nano-reinforced thermal conductive natural rubber composites, Polym. Compos. 37 (2016) 771–781. https://doi.org/10.1002/pc.23234.

[7] M.W. Ahmad, K. Soren, B. Dey, M.S. Khan, A. Choudhury, Synergistic reinforcement effect of 3D graphene@multi-walled carbon nanotube hybrid nanofiller in enhancing the electrical, EMI-shielding, and mechanical properties of polyethersulfone, Int. J. Polym. Anal. Charact. 26 (2021) 754–771. https://doi.org/10.1080/1023666X.2021.1976898.

[8] H.S. Kim, H.S. Bae, J. Yu, and S.Y. Kim, Thermal conductivity of polymer composites with the geometrical characteristics of graphene nanoplatelets, Sci. Rep. 6 (2016) 26825. https://doi.org/10.1038/srep26825.

[9] E.C. Cho, J.H. Huang, C.P. Li, C.W. Chang-Jian, K.C. Lee, Y. S. Hsiao, J.H. Huang, Graphene-based thermoplastic composites and their application for LED thermal management, Carbon N. Y. 102 (2016) 66–73. https://doi.org/10.1016/j.carbon.2016.01.097.

[10] Z. Han, A. Fina, Thermal conductivity of carbon nanotubes and their polymer nanocomposites: A review, Progress in Polymer Science (Oxford) 36 (2011) 914–944. https://doi.org/10.1016/j.progpolymsci.2010.11.004.

[11] F. Danafar, M. Kalantari, A Review of Natural Rubber Nanocomposites Based on Carbon Nanotubes, J. Rubber Res. 21 (2018) 293–310. https://doi.org/10.1007/BF03449176.

[12] S. Ata, C. Subramaniam, A. Nishizawa, T. Yamada, K. Hata, Highly Thermally Conductive Yet Flexible Composite of Carbon Fiber, Carbon Nanotube, and Rubber Obtained by Decreasing the Thermal Resistivity at the Interface between Carbon Fiber and Carbon Nanotube , Adv. Eng. Mater. 19 (2017) 1600596. https://doi.org/10.1002/adem.201600596.

[13] P.A. Klonos, S.N. Tegopoulos, C.S. Koutsiara, E. Kontou, P. Pissis, A. Kyritsis, Effects of CNTs on thermal transitions, thermal diffusivity and electrical conductivity in nanocomposites: comparison between an amorphous and a semicrystalline polymer matrix, Soft Matter 15 (2019) 1813–1824. https://doi.org/10.1039/C8SM02478B.

[14] A. Li, C. Zhang, Y.F. Zhang, Thermal Conductivity of Graphene-Polymer Composites: Mechanisms, Properties, and Applications, Polymers (Basel) 9 (2017) 437. https://doi.org/10.3390/polym9090437.

[15] B. Yin, J. Wang, H. Jia, J. He, X. Zhang, Z. Xu, Enhanced mechanical properties and thermal conductivity of styrene-butadiene rubber reinforced with polyvinylpyrrolidone-modified graphene oxide, J. Mater. Sci. 51 (2016) 5724–5737. https://doi.org/10.1007/s10853-016-9874-y.

[16] H. Yang, F. Cai, Y. Luo, X. Ye, C. Zhang, S. Wu, The interphase and thermal conductivity of graphene oxide/butadiene-styrene-vinyl pyridine rubber composites: A combined molecular simulation and experimental study, Compos. Sci. Technol. 188 (2020) 107971. https://doi.org/10.1016/j.compscitech.2019.107971.

[17] W. Liang, X. Ge, J. Ge, T. Li, T. Zhao, X. Chen, Y. Song, Y. Cui, M. Khan, J. Ji, X. Pang, R. Liu, Reduced Graphene Oxide Embedded with MQ Silicone Resin Nano-Aggregates for Silicone Rubber Composites with Enhanced Thermal Conductivity and Mechanical Performance, Polymers (Basel) 10 (2018) 1254. https://doi.org/10.3390/polym10111254.

[18] B. Zhong, Y. Luo, W. Chen, Y. Luo, D. Hu, H. Dong, Z. Jia, D. Jia, Immobilization of rubber additive on graphene for high-performance rubber composites, J. Colloid Interface Sci. 550 (2019) 190–198. https://doi.org/10.1016/j.jcis.2019.05.006.

[19] S.H. Song, J.M. Kimb, K.H. Parkc, D.J. Leee, O.S. Kwond, J. Kimb, H. Yoonb, X. Chena, High performance graphene embedded rubber composites, RSC Adv. 5 (2015) 81707–81712. https://doi.org/10.1039/C5RA16446J.

[20] S. Chen, Y. Feng, M. Qin, T. Ji, W. Feng, Improving thermal conductivity in the through-thickness direction of carbon fibre/SiC composites by growing vertically aligned carbon nanotubes, Carbon N. Y. 116 (2017) 84–93. https://doi.org/10.1016/j.carbon.2017.01.103.

[21] E. Pop, D. Mann, Q. Wang, K. Goodson, H. Dai, Thermal Conductance of an Individual Single-Wall Carbon Nanotube above Room Temperature, Nano Lett. 6 (2006) 96–100. https://doi.org/10.1021/nl052145f.

[22] S. Ghosh, I. Calizo, D. Teweldebrhan, E. P. Pokatilov, D. L. Nika, A. A. Balandin, W. Bao, F. Miao, C. N. Lau, Extremely high thermal conductivity of graphene: Prospects for thermal management applications in nanoelectronic circuits, Appl. Phys. Lett. 92 (2008) 151911. https://doi.org/10.1063/1.2907977.

[23] J.B. Donnet, Carbon black: science and technology, CRC Press, 1993.

[24] Y. Hu, G. Du, and N. Chen, A novel approach for Al2O3/epoxy composites with high strength and thermal conductivity, Compos. Sci. Technol. 124 (2016) 36–43. https://doi.org/10.1016/j.compscitech.2016.01.010.

[25] Y. Yao, X. Zeng, K. Guo, R. Sun, J. Xu, The effect of interfacial state on the thermal conductivity of functionalized Al2O3 filled glass fibers reinforced polymer composites, Compos. Part A Appl. Sci. Manuf. 69 (2015) 49–55. https://doi.org/10.1016/j.compositesa.2014.10.027.

[26] T. Zhou, X. Wang, G.U. Mingyuan, X. Liu, Study of the thermal conduction mechanism of nano-SiC/DGEBA/EMI-2,4 composites, Polymer (Guildf) 49 (2008) 4666–4672. https://doi.org/10.1016/j.polymer.2008.08.023.

[27] D. Shen, Z. Zhan, Z. Liu, Y. Cao, L. Zhou, Y. Liu, W. Dai, K. Nishimura, C. Li, C.T. Lin, N. Jiang, J. Yu, Enhanced thermal conductivity of epoxy composites filled with silicon carbide nanowires, Sci. Rep. 7 (2017) 2606. https://doi.org/10.1038/s41598-017-02929-0.

[28] C. Jiang, D. Zhang, X. Gan, R. Xie, F. Zhang, K. Zhou, Preparation of high performance AlN/Hydantion composite by gelcasting and infiltration processes, Ceram. Int. 40 (2014) 2535–2538. https://doi.org/10.1016/j.ceramint.2013.07.131.

[29] A. Ma, W. Chen, Y. Hou, G. Zhang, The Preparation and Cure Kinetics Researches of Thermal Conductivity Epoxy/AlN Composites, Polym. Plast. Technol. Eng. 49 (2010) 354–358. https://doi.org/10.1080/03602550903532091.

[30] H. Fang, S.-L. Bai, C.P. Wong, 'White graphene' – hexagonal boron nitride based polymeric composites and their application in thermal management, Compos. Commun. 2 (2016) 19–24. https://doi.org/10.1016/j.coco.2016.10.002.

[31] A. K. Srivastava, Oxide nanostructures: growth, microstructures, and properties. CRC Press, 2014.

[32] K. Wefers, C. Misra, Oxides and hydroxides of aluminum, Pittsburgh: Alcoa Laboratories, 1987.

[33] R.J. Warzoha, A.S. Fleischer, Heat flow at nanoparticle interfaces, Nano Energy 6 (2014) 137–158. https://doi.org/10.1016/j.nanoen.2014.03.014.

[34] Y. Ouyang, L. Bai, H. Tian, X. Li, F. Yuan, Recent progress of thermal conductive polymer composites: Al_2O_3 fillers, properties and applications, Compos. Part A Appl. Sci. Manuf. 152 (2022) 106685. https://doi.org/10.1016/j.compositesa.2021.106685.

[35] R. Scotti, L. Conzatti, M. D'Arienzo, B. Di Credico, L. Giannini, T. Hanel, P. Stagnaro, A. Susanna, L. Tadiello, F. Morazzoni, Shape controlled spherical (0D) and rod-like (1D) silica nanoparticles in silica/styrene butadiene rubber nanocomposites: role of the particle morphology on the filler reinforcing effect, Polymer 55 (2014) 1497–1506. https://doi.org/10.1016/j.polymer.2014.01.025.

[36] B. Credico, E. Cobani, E. Callone, L. Conzatti, D. Cristofori, M. D'Arienzo, S. Dirè, L. Giannini, T. Hanel, R. Scotti, P. Stagnaro, L. Tadiello, F. Morazzoni, Size-controlled self-assembly of anisotropic sepiolite fibers in rubber nanocomposites, Applied Clay Science 152 (2018) 51-64. https://doi.org/10.1016/j.clay.2017.10.032.

[37] D.B. Cordes, P.D. Lickiss, F. Rataboul, Recent Developments in the Chemistry of Cubic Polyhedral Oligosilsesquioxanes, Chem. Rev. 110 (2010) 2081–2173. https://doi/10.1021/cr900201r.

[38] X. Huang, C. Zhi, P. Jiang, D. Golberg, Y. Bando, T. Tanaka, Polyhedral Oligosilsesquioxane-Modified Boron Nitride Nanotube Based Epoxy Nanocomposites: An Ideal Dielectric Material with High Thermal Conductivity, Adv. Funct. Mater. 23 (2013) 1824–1831. https://doi.org/10.1002/adfm.201201824.

[39] J. Gu, C. Liang, J. Dang, W. Dong, Q. Zhang, Ideal dielectric thermally conductive bismaleimide nanocomposites filled with polyhedral oligomeric silsesquioxane functionalized nanosized boron nitride, RSC Adv. 6 (2016) 35809–35814. https://doi.org/10.1039/C6RA04513H.

[40] J. Gu, Y. Guo, Z. Lv, W. Geng, Q. Zhang, Highly thermally conductive POSS-g-SiCp/UHMWPE composites with excellent dielectric properties and thermal stabilities, Compos. Part A Appl. Sci. Manuf. 78 (2015) 95–101. https://doi.org/10.1016/j.compositesa.2015.08.004.

[41] M. D'Arienzo, M. Redaelli, E. Callone, L. Conzatti, B. Di Credico, S. Dirè, L. Giannini, S. Polizzi, I. Schizzi, R. Scotti, L. Tadiello, F. Morazzoni, Hybrid SiO_2@POSS nanofiller: a promising reinforcing system for rubber nanocomposites, Mater. Chem. Front. 1 (2017) 1441–1452. https://doi.org/10.1039/C7QM00045F

[42] L. Tadiello, L. Giannini, T. Hanel, M., M. D'Arienzo, B. Di Credico, R. Scotti, F. Morazzoni US Patent 11091607. 2021

[43] M. Redaelli, M. D'Arienzo, J. Brus, B. Di Credico, M. Geppi, L. Giannini, L. Matejka, F. Martini, F. Panattoni, M. Spirkova, M. Slouf, R. Scotti, F. Morazzoni, On the key role of SiO2@POSS hybrid filler in tailoring networking and interfaces in rubber nanocomposites, Polym. Test. 65 (2018) 429–439. https://doi.org/10.1016/j.polymertesting.2017.12.022.

[44] K. Numata, H. Kurokawa, S. Sekine, Y. Nakazawa, A. Asano, Determination of limiting values of 1H spin-spin relaxation time to assess lifetime of thermally aged acrylonitrile butadiene rubber, Polym. Degrad. Stab. 162 (2019) 12–21. https://doi.org/10.1016/j.polymdegradstab.2019.02.004.

[45] P. Tarte, Infra-red spectra of inorganic aluminates and characteristic vibrational frequencies of AlO4 tetrahedra and AlO6 octahedra, Spectrochim. Acta Part A Mol. Spectrosc. 23 (1967) 2127–2143. https://doi.org/10.1016/0584-8539(67)80100-4.

[46] M. Fedel, E. Callone, S. Diré, F. Deflorian, M.-G. Olivier, M. Poelman, Effect of Na-Montmorillonite sonication on the protective properties of hybrid silica coatings, Electrochim. Acta 124 (2014) 90–99. https://doi.org/10.1016/j.electacta.2013.11.006.

[47] T. Takahashi, T. Ohkubo, K. Suzuki, Y. Ikeda, High resolution solid-state NMR studies on dissolution and alteration of Na-montmorillonite under highly alkaline conditions, Microporous Mesoporous Mater. 106 (2007) 284–297. https://doi.org/10.1016/j.micromeso.2007.03.008.

[48] S. Borsacchi, U.P. Sudhakaran, L. Calucci, F. Martini, E. Carignani, M. Messori, M. Geppi, Rubber-Filler Interactions in Polyisoprene Filled with In Situ Generated Silica: A Solid State NMR Study, Polymers (Basel) 10 (2018) 822. https://doi.org/10.3390/polym10080822.

[49] Y.Ouyang, X. Li, F. Ding, L. Bai, F. Yuan, Simultaneously enhance thermal conductive property and mechanical properties of silicon rubber composites by introducing ultrafine Al2O3 nanospheres prepared via thermal plasma, Composites Science and Technology 190 (2020) 1-10. https://doi.org/10.1016/j.compscitech.2020.108019

[50] B.Z. Gao, J.Z. Xu, J.J. Peng, F.Y. Kanga, H.D. Du, J. Li, S.W. Chiang, C.J. Xu, N. Hu, X.S. Ning, Experimental and theoretical studies of effective thermal conductivity of composites made of silicone rubber and Al2O3 particles, Thermochimica Acta 614 (2015) 1-8. https://doi.org/10.1016/j.tca.2015.06.005.

[51] L. Tadiello, M. D'Arienzo, B. Di Credico, T. Hanel, L. Matejka, M. Mauri, F. Morazzoni, R. Simonutti, M. Spirkova, R. Scotti, The filler–rubber interface in styrene butadiene nanocomposites with anisotropic silica particles: morphology and dynamic properties, Soft Matter 11 (2015) 4022-4033. https://doi.org/10.1039/C5SM00536A.